TRAVEL DISTANCE AND EXTENT DEPOSITION OF MOTION OF DEBRIS FLOW AS EFFECT OF SOIL POROSITY

M. Mukhlisin
Jurusan Teknik Sipil Politeknik Negeri Semarang

Abstract

Factors affecting the behavior of debris flow run-out include source material composition, volume of initial failure, slope angle at source, source slope morphology, degree of saturation of initial failure material, the type, depth and degree of saturation of path material, presence of surface water in slide path, vegetation along run-out path, and path confinement. The effective soil porosity is expected to have a great effect on some of these factors. Although many studies using a numerical simulation have been performed to analyze debris flow run-out, the effect of ESP (Effective Soil Porosity) has not been considered as a main contributor to the length of debris flow run-out. Therefore, this study examines the effect of ESP variation on travel distance of debris flow run-out. The results demonstrate that ESP is a dominant factor in determining the travel distance and the distribution of debris flow; that is, when the slope had a larger ESP value, the slope had greater water content in the sliding segment, resulting in a faster and longer travel distance, as well as in a broader distribution of debris flow. Consequently, a larger ESP value may increase the risk of damage in the downstream region.

Keywords*:* Effective Soil Porosity, travel distance, debris flow run-out

1. INTRODUCTION

The prediction of debris flow run-out is an essential component of landslide hazard assessment. Many studies have used numerical simulations (*e.g.*, Hungr, 1995; Chen and Lee, 2000; Laigle *et al.*, 2003, Ghilardi *et al.*, 2003), and all have confirmed that the prediction of debris flow run-out is required to identify the hazard area of a potential landslide and to map the potential extent of deposition based on hazard intensity parameters such as velocity, flow depth, and thickness of the deposits.

The pre-failure factors affecting the behavior of debris flow run-out include source material composition; volume of initial failure; slope angle at the source; source slope morphology; degree of saturation of the initial failure material; the type, depth, and degree of saturation of the path material; the presence of surface water in the slide path; vegetation along the run-out path; and path confinement (Ayotte and Hungr, 2000; Okura *et al.*, 2003). The run-out parameters include the maximum distance the discharge has reached, flow velocities, the thickness and scope of deposition, and the behavior of the flow at bends and obstacles in the flow path (Hungr, 1995).

Mukhlisin et al (2006) discussed a numerical simulation for analyzing rainwater infiltration on unsaturated soil and its effect on slope stability through the variation in effective soil porosity (ESP). ESP values were found have a significant effect on the timing of discharge and increases in pore water pressure, thereby controlling the timing of slope failure. A greater ESP value tends to increase the water content of the corrupted matter. In the event that slope failure occurs and evolves into debris flow, it may contribute to a longer travel distance of the debris flow run-out, and greater damage may therefore be expected in the downstream region. Therefore, a thorough analysis of the effect of ESP variation on travel distance and the extent of deposition of the debris flow run-out is vital; this is the main focus of this study.

2. METHOD OF NUMERICAL STUDY

According Nakagawa *et al.* (2000), debris flow deposits such as the Harihara landslide deposit generally consist of two layers: the lower, undisturbed earth-block layer (*i.e.*, the original ground layer including surface soil, trees, and roots) and the upper, disturbed deposit layer. During a landslide, the solid earth block descends first, followed by the debris flow deposits that settle over the block. To analyze the effect of variation in ESP on this phenomenon, this study investigates a two-dimensional numerical model of the finite difference method for the movement of debris flow. The computer program of this numerical model was developed by Satofuka and Takahashi (2003).

2.1. Debris flow motion

As in Takahashi *et al.* (2003), the numerical model was based upon the Eulerian continuous fluid equation, and the motion of the solid earth block was analyzed as a point of mass in a Lagrangian treatment.

The continuity equation of the liquid layer is

$$\frac{\partial h}{\partial t}+\frac{\partial uh}{\partial x}+\frac{\partial vh}{\partial y}-i_s=0 \tag{1}$$

and the equations of liquid layer motion toward the x and y directions are, respectively,

$$\frac{\partial u}{\partial t}+u\frac{\partial u}{\partial x}+v\frac{\partial u}{\partial y}=g\sin\alpha_{wx}-\frac{\tau_{sx}}{\rho_T h}-\frac{\tau_{bx}}{\rho_T h} \tag{2}$$

$$\frac{\partial v}{\partial t}+u\frac{\partial v}{\partial x}+v\frac{\partial v}{\partial y}=g\sin\alpha_{wy}-\frac{\tau_{sy}}{\rho_T h}-\frac{\tau_{by}}{\rho_T h} \tag{3}$$

where u and v are velocities toward x and y, respectively; h is the thickness of the liquid layer; t is time; i_s is the rate at which a solid earth block transforms into a liquid layer; τ_{sx} and τ_{sy} are x- and y-wise shear stresses working on the boundary between the earth block and the liquid layer (the upper boundary); τ_{bx} and τ_{by} are x- and y-wise shear stresses working on the boundary between the liquid layer and the bottom layer of flow (the lower boundary); α_{xy}, α_{wy} are x- and y-wise gradients of the earth-block surface; g is gravitational acceleration, ρ_T is the density of liquids $(=C\rho_s+(1-C)\rho_w)$; C is the concentration of solids in the liquid by volume; ρ_s is the density of solids; and ρ_w is the density of water.

The boundary shear stresses in equations 2 and 3 are given by Takahashi *et al.* (2000) as

$$\frac{\tau_{sx}}{\rho_T h}=\frac{9\mu_a{}^2(u-u_b)\sqrt{(u-u_b)^2+(v-v_b)^2}}{\rho_T{}^2 gh^4\left|\sin\alpha_w\right|} \tag{4}$$

$$\frac{\tau_{sy}}{\rho_T h}=\frac{9\mu_a{}^2(v-v_b)\sqrt{(u-u_b)^2+(v-v_b)^2}}{\rho_T{}^2 gh^4\left|\sin\alpha_w\right|} \tag{5}$$

$$\frac{\tau_{bx}}{\rho_T h}=\frac{9\mu_a{}^2 u\sqrt{u^2+v^2}}{\rho_T{}^2 gh^4\left|\sin\alpha_w\right|} \tag{6}$$

$$\frac{\tau_{by}}{\rho_T h}=\frac{9\mu_a{}^2 v\sqrt{u^2+v^2}}{\rho_T{}^2 gh^4\left|\sin\alpha_w\right|} \tag{7}$$

where μ_a is the apparent viscosity of the liquid layer, u_b and v_b are the x- and y-wise velocities of the earth block, and α_w is the surface gradient of the earth block as given by

$$\left|\sin\alpha_w\right|=\sqrt{(\sin\alpha_{wx})^2+(\sin\alpha_{wx})^2} \tag{8}$$

The moving earth block in the initial state is considered to be an array of cylinders standing perpendicular to the bed and arranged in contact with each other in tetrahedral-rectangular rows. To compensate for the void space between three adjacent cylinders, these cylinders are considered to overlap each other at the contact area as shown in Figure 1. If the distance between the centers of two adjacent cylinders of uniform diameter is D, the diameter of each cylinder should be about 1.05 D_1 (=2r). This model of arranged cylinders is adopted to avoid the complicated calculation of rotating motions of dispersed earth blocks.

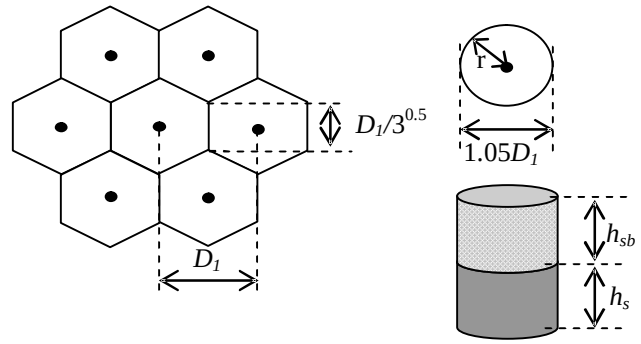

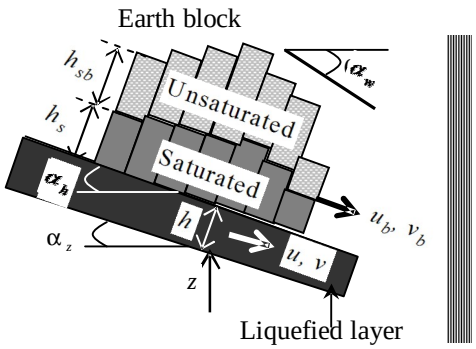

Figure 1. Plan and side views of the liquefied layer and the earth block as an array of cylinders.

A cylinder that is supported by the liquefied layer is considered to be composed of a lower layer of saturated water and an upper, unsaturated (degree of saturation, S_b) layer; and the thicknesses of these layers are h_s and $h_{sb,}$ respectively. Therefore, the mass of a cylinder M_b is given by

$$M_b = \rho_T S_0 (\delta_1 h_{sb} + h_s) \tag{9}$$

where

$$\delta_1 = \{C\rho_s + (1-C)\rho_w S_b\} / \{C\rho_s + (1-C)\rho_w\},$$

in which S_o is the bottom area of the cylinder, and the solid concentrations in the saturated layer, the unsaturated layer, and the liquid layer are all considered to be equal.

The *x*- and *y*-wise equations of a cylinder are

$$\frac{\partial u_b}{\partial t} = g \sin\alpha_x + \frac{\tau_{sx} S_0}{M_b} + \frac{1}{M_b}\{\sum f_x + \sum f_{xs}\} \tag{10}$$

$$\frac{\partial v_b}{\partial t} = g \sin\alpha_y + \frac{\tau_{sy} S_0}{M_b} + \frac{1}{M_b}\{\sum f_y + \sum f_{ys}\} \tag{11}$$

where α_x and α_y are the *x*- and *y*-wise gradients of the liquid layer surface (if the liquid layer does not exist, then they are the gradients of the bottom layer); f_x and f_y are *x*- and *y*-wise attractive or repulsive forces working between the cylinders; and f_{xs} and f_{ys} are *x*- and *y*-wise shear stress fractions between the cylinders.

The rate of liquefaction from the lower layer of the cylinder is given by Takahashi (2000) as

$$i_s = \beta_s \sqrt{(u-u_b)^2 + (v-v_b)^2} \tag{12}$$

Liquefaction proceeds as long as the saturated layer exists in the lower part of a cylinder, but it does not occur in the unsaturated layer.

2.2. Soil parameters

The finite difference representation of the fundamental equation above is used to simulate the motion of debris flow. The grid mesh for the calculation of debris flow is a square with 100-cm sides, and the time increment is 0.001 seconds. The radii of the earth-block cylinder *r* for 40° and 35° slope gradients are set at 30.771 cm and 33.297 cm, and the values of D_1 are set at 58.61 cm and 63.42 cm, respectively. As a result, there are 20 earth-block cylinders in any cross section of the sliding segment slope failure in either slope gradient, while the longitudinal sections include ten earth-block cylinders. Furthermore, the density values of solids and water are 2.65 g/cm^3 for solids and 1.00 g/cm^3 for water.

The main parameters for this analysis are the thickness of the saturated earth block, h_{sb}, and the thickness of the unsaturated earth block, h_s, in the sliding segment of the slope; the degree of saturation, S_b, in the unsaturated segment of the earth block; and the sediment concentrations in the liquid layer and earth block, *C*. The liquefied layer was assumed to

be 1.00 cm deep, at which point the apparent viscosity, μ_a, is affected by the sediment concentration, *C* (Lorenzini and Mazza 2004).

2.2.1. Soil thickness

The thickness of the unsaturated and saturated soil layers in the sliding segment of slope is illustrated in Fig. 2a-c.

Figure 2 shows that the thicknesses of the saturated and unsaturated soils in the sliding segment of slope failure are similar in cases 1, 2, and 3 in each scenario. In addition, the total depth of slope failure is similar in scenarios 1, 2, and 3.

Scenarios 1 and 2, which shared the same slope gradient of 40°, showed similar thicknesses of saturated and unsaturated layers at the estimated time of slope failure (see Fig. 2a-b). However, scenario 3, which had a 35° slope gradient, showed a deeper saturated soil layer and a shallower unsaturated soil layer in the sliding segment of the slope compared to scenarios 1 and 2 (Fig. 2c).

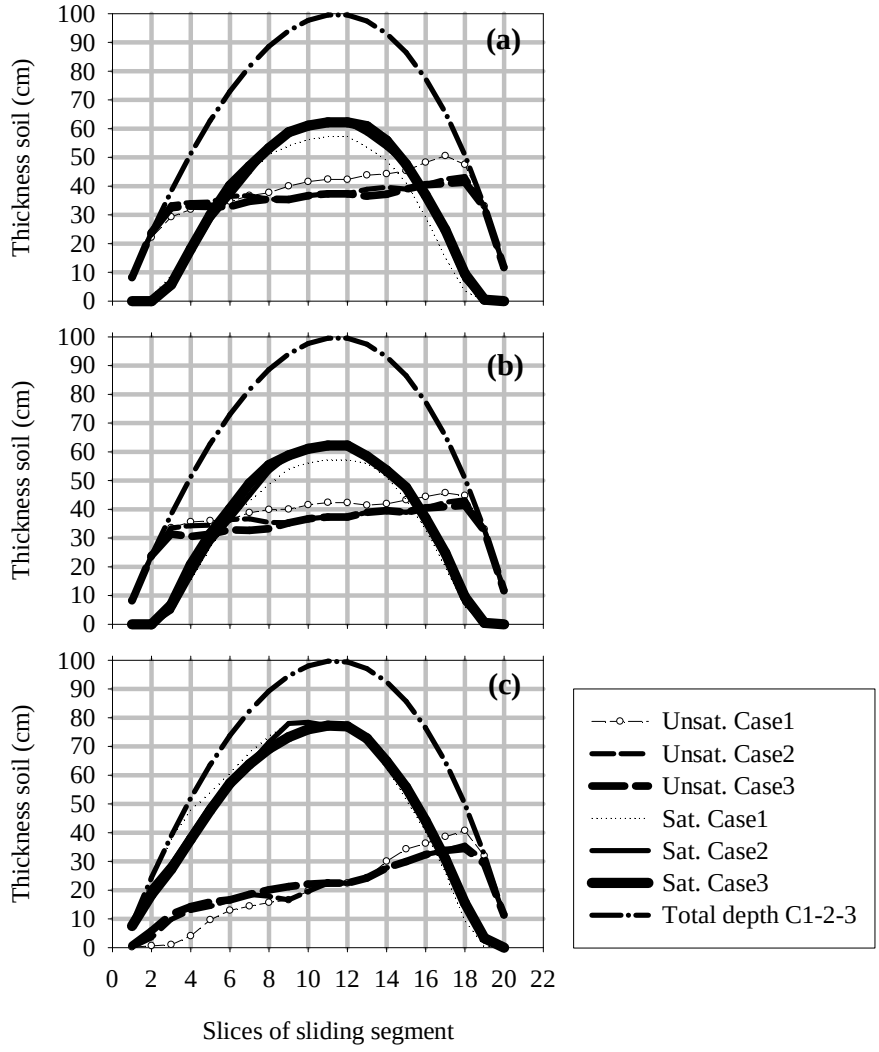

Figure 2. Soil thicknesses of the unsaturated and saturated layers and total depth for cases 1, 2, and 3 in the sliding segment of slope for (a) scenario 1, (b) scenario 2, and (c) scenario 3 of the analysis model.

2.2.2. Degree of saturation

As shown in Fig. 3a-c, the degree of saturation, S_b, in the unsaturated part of the earth block is similar in each case for scenarios 1, 2, and 3. The relatively larger value of S_b

when slope failure occurred (*i.e.*, when $Fs < 1$) indicates that the unsaturated part of the earth block was in a wetter condition.

The similar degrees of saturation in each case for scenarios 1, 2, and 3 indicate that neither ESP variations nor slope gradient variations (40^o and 35^o) have an effect on the degree of saturation.

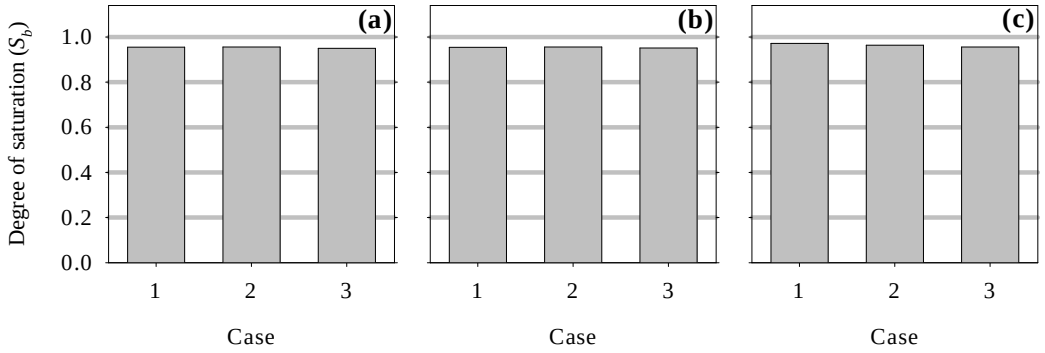

Figure 3. Degree of saturation in the unsaturated part of the earth block for (a) scenario 1, (b) scenario 2, and (c) scenario 3 in cases 1, 2, and 3.

2.2.3. Sediment concentration

Figure 4a-c shows the sediment concentration in cases 1, 2, and 3 in scenarios 1, 2, and 3. In each scenario, case 1 has a smaller ESP value, resulting in a higher sediment concentration than in case 2, because a relatively smaller ESP value results in the surface layer having a relatively smaller water-holding capacity. In contrast, case 3 has a larger ESP value, resulting in a smaller sediment concentration than in case 2, because a relatively greater ESP value results in the surface layer having a relatively greater water-holding capacity.

Figure 4a and c shows the similar sediment concentrations shared by scenarios 1 and 3 in cases 1, 2, and 3, which are attributable to similar ESP variations in the surface layers and fixed ESP values in the sub-surface layers. However, scenario 2 shows a higher sediment concentration for case 1, similar concentrations for case 2, and lower sediment concentrations for case 3 than those shown in scenarios 1 and 3, due to the ESP variations within both the surface and sub-surface layers in scenario 2.

The input data used in this study are the concentrations of sediment in the earth block and liquid layers. Sediment concentration in the earth block, as shown in Fig. 4a-c, was obtained from the stability of slope analysis, whereas the sediment concentration value of 1.00 cm for the liquid layer in the sliding segment was assumed to be similar in the earth block at the estimated time of slope failure.

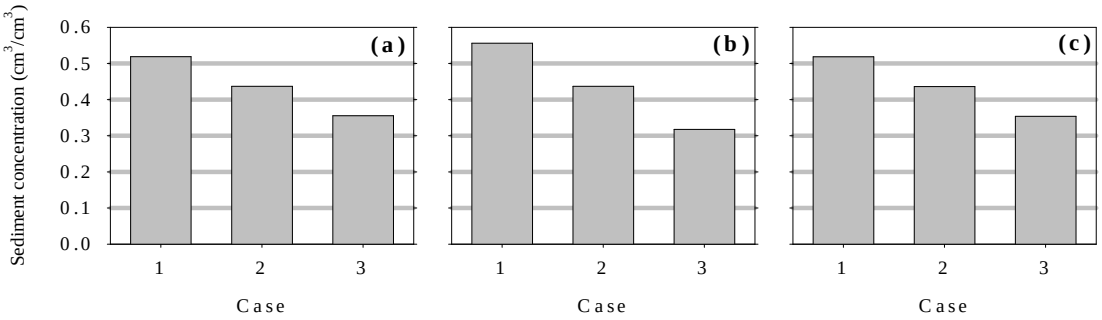

Figure 4. Volumetric sediment concentrations in cases 1, 2, and 3 in the sliding segment of the slope for (a) scenario 1, (b) scenario 2, and (c) scenario 3.

2.3. General geometry of the slope topography

Almost every slope stability analysis incorporates the influence of rainfall on changing groundwater flow patterns, such as increasing pressure heads and often a rising groundwater table, as shown in Fig. 5b. The geometry of slope failure as shown in Fig. 5a simulates the actual situation in which slope failure occurs in the sliding segment along the slip surface simultaneously with the elevation of the ground water table in the slope (see Fig. 5b).

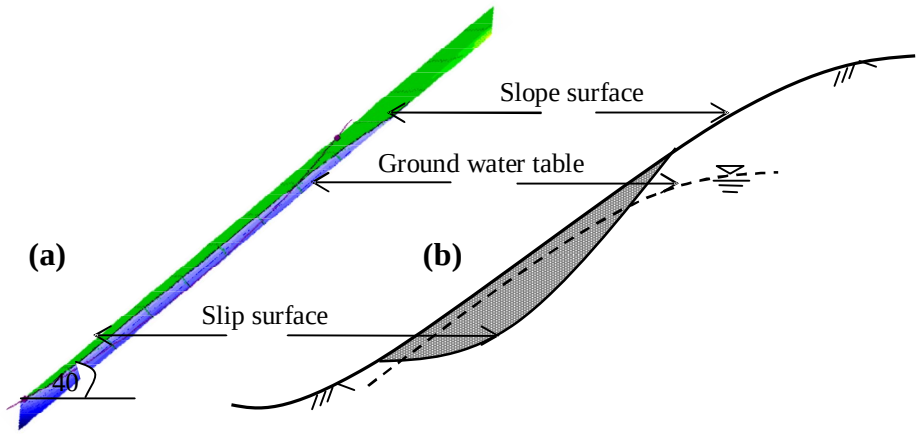

Figure 5. The earth mass begins moving in (a) the simulation model and (b) the actual situation.

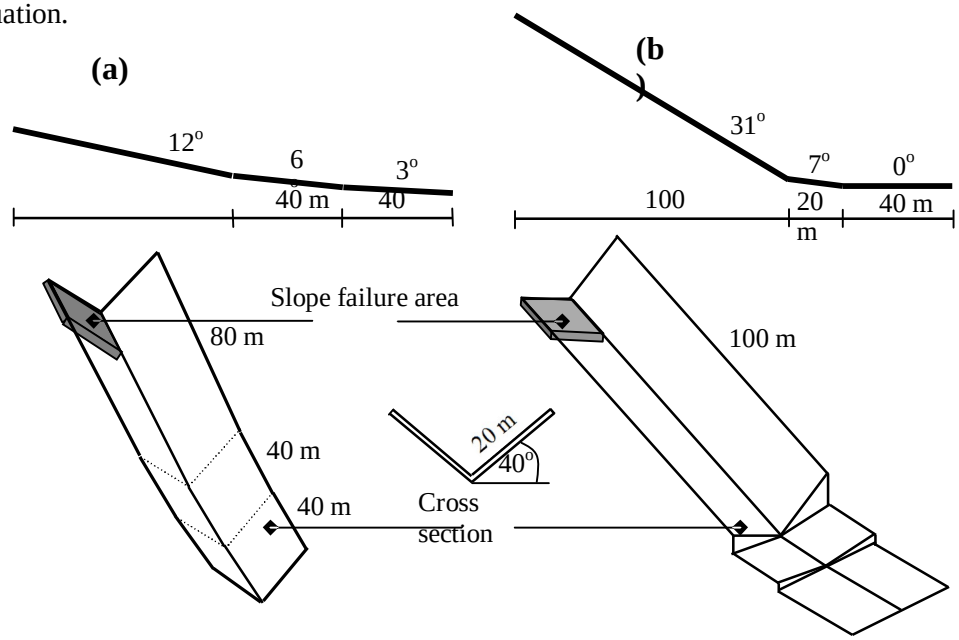

Figure 6. A longitudinal section of the simulation model for (a) long run-out and (b) extent of deposition.

To analyze the effect of ESP variation on the travel distance and extent of deposition of debris flow, two types of topography (Fig. 6a and b) were examined. The longitudinal section used for run-out analysis comprises lengths of 80, 40, and 40 m, with 12^o, 6^o, and 3^o slope gradients (Fig. 6a), and the longitudinal section for the deposition analysis comprises lengths of 100, 20, and 40 m, with 31^o, 7^o, and 0^o slope gradients (Fig. 6b).

The slope failure area was assumed to be located near the top of the longitudinal

section in both of the simulation models, as the slope gradients for both cross sections were quite similar, *i.e.*, 40° in one case and 35° in the other (see Fig. 6a and b).

2.4. Scenarios for the numerical simulation

Three scenarios of the effect of soil porosity on the travel distance and extent of deposition of debris flow run-out were evaluated. The initial conditions of these three scenarios were the same at the estimated time of slope failure. The scenarios of the simulation analysis are summarized in Table 1.

The parameters in scenario 1, as summarized in Table 1, were used for the simulation model. The parameters included were a 100-cm depth of soil, 2000-cm length of slope, and a 40° slope gradient. In scenario 1, the ESP variations used for cases 1, 2, and 3 were applied to the surface layer, while the ESP value for the sub-surface layer was fixed at the same value as in case 2.

In scenario 2, the ESP variations in cases 1, 2, and 3 were applied to both the surface and the sub-surface layers, and the only difference in scenario 1 was the change in the soil porosity of the surface layer. However, the other parameters used were the same as those applied in scenario 1 (*i.e.*, 100-cm depth, 2000-cm length, and a 40° slope gradient).

Table 1. Summary of the simulation analysis of the effect of ESP variation on travel distance and extent of deposition of debris flow run-out.

Sce-nario No.	Soil thickness (cm)	Slope gradient (degree)	Soil porosity change	Cases	Debris flow run-out analyzed
1-a	100	40	Surface	1, 2, 3	Travel distance
1-b	100	40	Surface	1, 2, 3	Extent of deposition
2-a	100	40	Surface and sub-surface	1, 2, 3	Travel distance
2-b	100	40	Surface and sub-surface	1, 2, 3	Extent of deposition
3-a	100	35	Surface	1, 2, 3	Travel distance
3-b	100	35	Surface	1, 2, 3	Extent of deposition

In scenario 3, the same parameters were applied as in scenario 1 except for one parameter change: the slope gradient was changed from 40° to 35°. In this scenario, the effect of the change in slope gradient was analyzed with respect to the variation in soil porosity as in scenario 1. In each scenario, the effect of the soil porosity variation on the travel distance and extent of deposition of debris flow run-out was analyzed, as summarized in Table 1.

3. RESULTS

The source area of slope failure in a sliding segment, as shown in 6, was assumed to be in the upper part of the channel in all cases (see Figs. 6a-b and 7). Figure 7 shows the area of the slope failure at time = 0.00 seconds. In the sliding segment of slope failure (Fig. 7), there are 20 earth block cylinders in the cross section and ten in the longitudinal section of the slope channel.

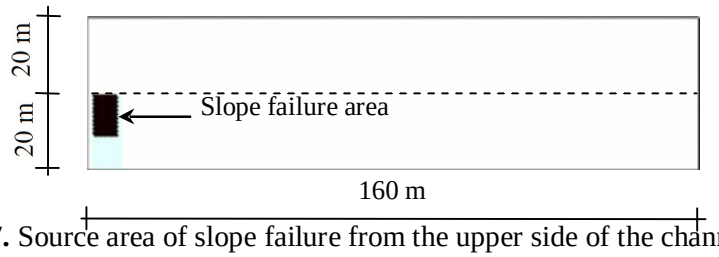

Figure 7. Source area of slope failure from the upper side of the channel in simulations of both travel distance and extent of deposition of debris flow at time = 0.00 seconds.

3.1. Influence of soil porosity of the surface layer (scenario 1)

3.1.1 Travel distance in scenario 1

In scenario 1, the parameters of soil depth (100 cm), slope length (2000 cm), and slope gradient (40^o) were applied in the analysis of travel distance and extent of deposition of debris flow run-out in response to variations in ESP values. In this scenario, the ESP variations defined in cases 1, 2, and 3 were applied to the surface layer, while soil porosity values for the sub-surface layer were fixed at the same value as in case 2 (see scenario 1, Table 1).

Figure 8a-c shows the effect of ESP variation on the travel distance of debris flow run-out in cases 1, 2, and 3. Figure 8b shows that in case 2, the earth block of debris flow at time = 50.0 seconds has traveled about 87.46 m from the top of a channel with a 6^o slope gradient. In case 1, which has a smaller ESP value than case 2, the motion of debris flow is very slow, and at time = 50.0 seconds, the earth block of debris flow has traveled only about 49.70 m from the top of a channel with a 12^o slope gradient (Fig. 8a), because the smaller ESP value results in a larger concentration of sediment in the surface layer (Fig. 4a).

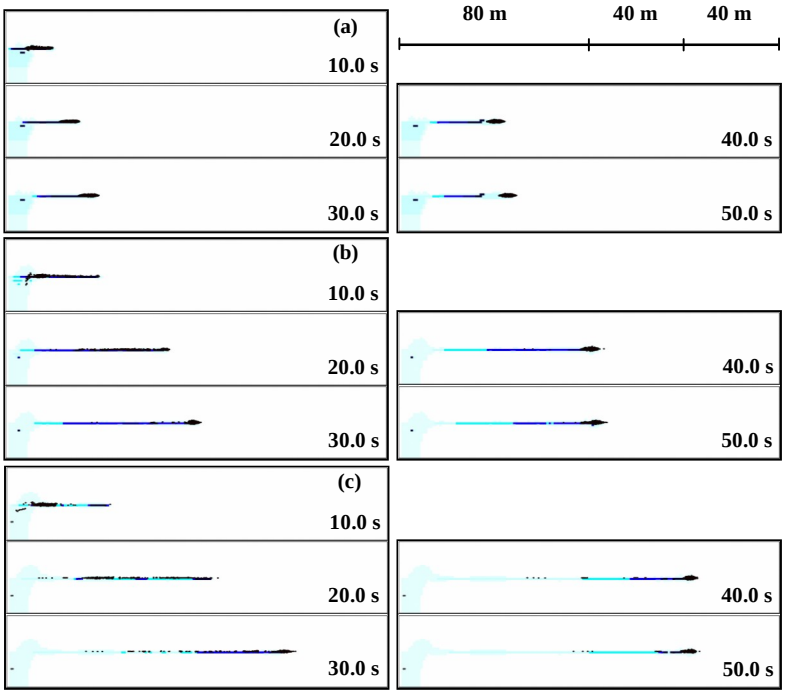

Figure 8 Effect of ESP variation on the travel distance of debris flow in scenario 1 for (a) case 1, (b) case 2, and (c) case 3.

In case 3, which has a greater ESP value than case 2, the motion of debris flow is faster. At time = 50.0 seconds, the earth block of debris flow has traveled about 126.39 m from the top of a channel with a slope gradient of 3^o (Fig. 8c), because the relatively greater ESP value results in a smaller concentration of sediment in the surface layer (Fig. 4a).

These results demonstrate that the ESP value has a significant effect on the run-out distance of debris flow, in that a relatively larger ESP value results in a relatively smaller concentration of sediment in the sliding segment, resulting in a debris flow that travels faster and over a longer distance.

3.1.2 Extent of deposition in scenario 1

Figure 9 shows the spread of debris flow deposition in response to ESP variations in the surface layer. Figure 9a-c shows that the earth block descends quickly in the first 100 m in all cases due to the steepness of the channel slope. The figure also shows that the earth block cylinder reaches the deposition area more rapidly than the liquid layer that follows it. The deposition areas covered by the earth block of debris flow differ in each case as a result of the variations in ESP values.

In case 1, which has a smaller ESP value than case 2, the deposition of the earth block of debris flow on a slope gradient of 7^o is located about 120 m from the top channel at time = 50.0 seconds (see Fig. 9a). However, in case 3, which has a larger ESP than case 2, the deposition of the earth block of debris flow spreads farther and wider, as the deposit is located more than 120 m from the top of a channel with a slop gradient of 0^o (see Fig. 9c).

These results suggest that ESP values are also a dominant factor in determining the extent of deposition of the debris flow, in that relatively larger ESP values result in a broader area of debris flow deposition, which may cause greater levels of damage in the downstream area of a landslide.

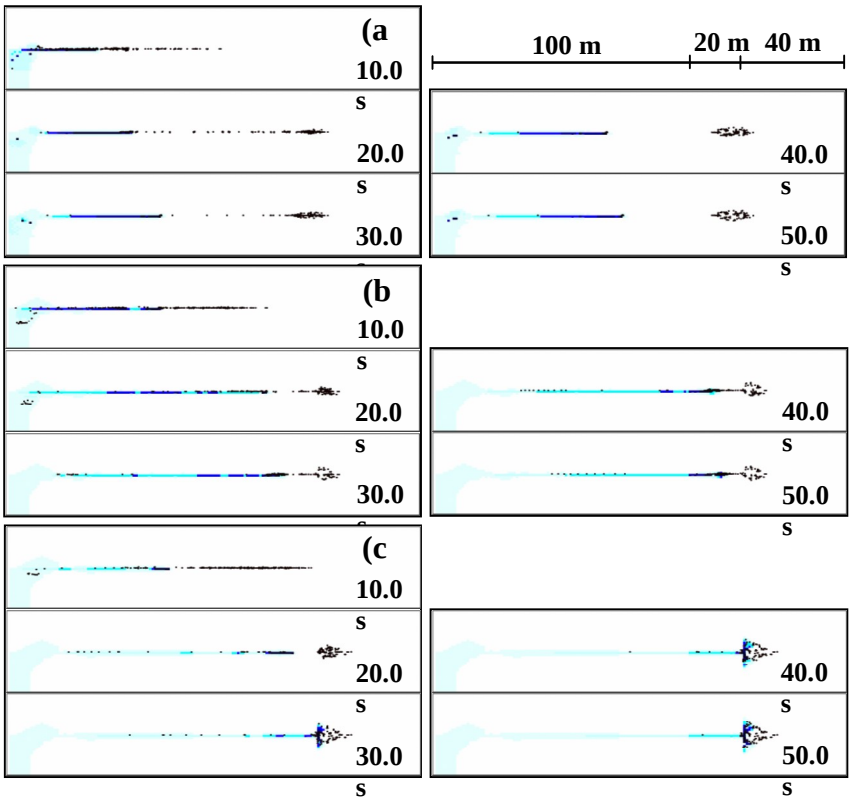

Figure 9. Effect of ESP variation on the extent of deposition of debris flow in scenario 1 for (a) case 1, (b) case 2, and (c) case 3.

3.2. Influence of the soil porosity of both surface and sub-surface layers (scenario 2)

3.2.1 Travel distance in scenario 2

In scenario 2, variations in ESP were analyzed in both the surface and sub-surface layers. All parameters used in scenario 2 were the same as those used in scenario 1, except for a variation in the soil porosity value of the surface layer.

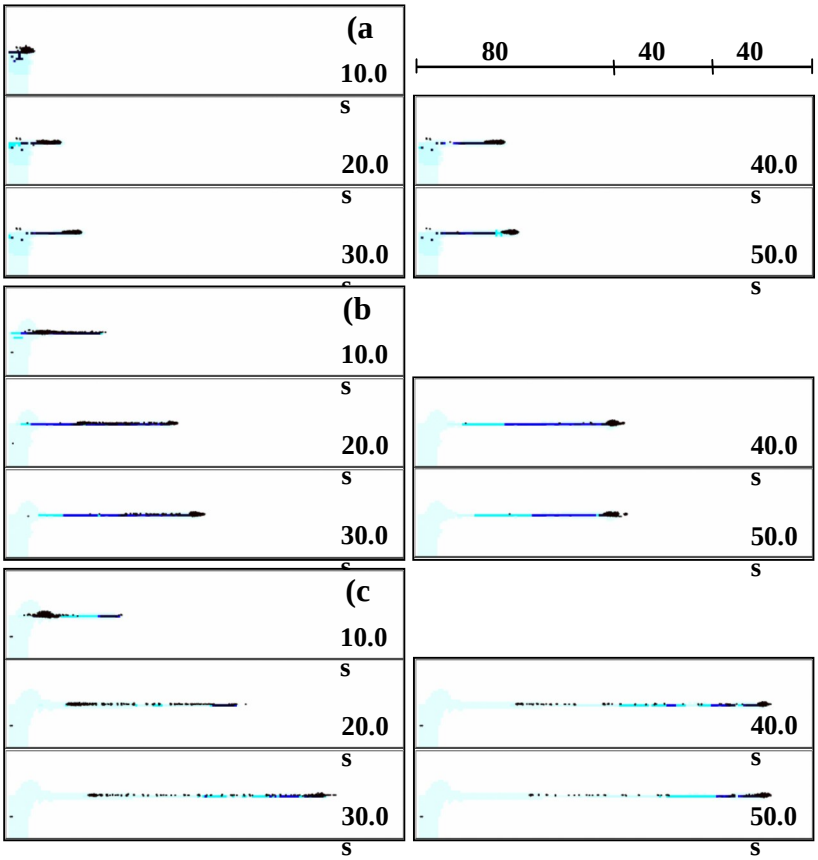

Figure 10. Effect of variations in ESP on the travel distance of debris flow in scenario 2 for (a) case 1, (b) case 2, and (c) case 3.

An analysis of ESP variation in the surface and sub-surface layers showed that when slope failure occurred, scenario 2 experienced a greater sediment concentration than scenario 1, case 1; a similar sediment concentration to scenario 1, case 2; and lower sediment concentrations than in scenario 1, case 3 (see Fig. 4a-b). The thickness and degree of saturation of the saturated and unsaturated earth blocks were similar for all cases in scenarios 1 and 2 (Figs. 2a-b and 3a-b).

Figures 10 and 11 show that the general trends in the effect of variations in ESP on travel distance and extent of deposition of debris flow run-out are similar in scenarios 1 and 2. Comparisons between the analyses of scenarios 1 and 2 demonstrate that scenario 2 had a shorter travel distance of debris flow in case 1, similar travel distance in case 2, and a longer travel distance in case 3 than the same cases in scenario 1 (see Figs. 8 and 10). This is due to the effect of sediment concentrations in scenario 2, which are greater in case 1, similar in case 2, and smaller in case 3 than those in the same cases of scenario 1 (see Fig. 4a-b). In scenario 2, the maximum travel distance of debris flow, as shown in Fig. 10a-c, is about 41.61 m, 85.35 m, and 143.77 m from the top of the channel for cases 1, 2, and 3, respectively.

3.2.2. Extent of deposition in scenario 2

Figure 11 shows the extent of deposition of debris flow for cases 1, 2, and 3 in scenario 2. Case 1, which has a smaller ESP value than case 2, showed a smaller extent of deposition, while case 3, with a greater ESP value than case 2, showed a wider extent of deposition. Moreover, a comparison between scenarios 1 and 2 shows that in scenario 2, the extent of the deposition of debris flow was relatively smaller for case 1, similar for case 2, and greater for case 3 than the same cases in scenario 1 (see Figs. 9 and 11). These results also demonstrate that the ESP value has a significant effect on the travel distance and the extent of deposition of debris flow, in that larger ESP values result in a faster and longer travel distance and in a broader extent of debris flow deposition.

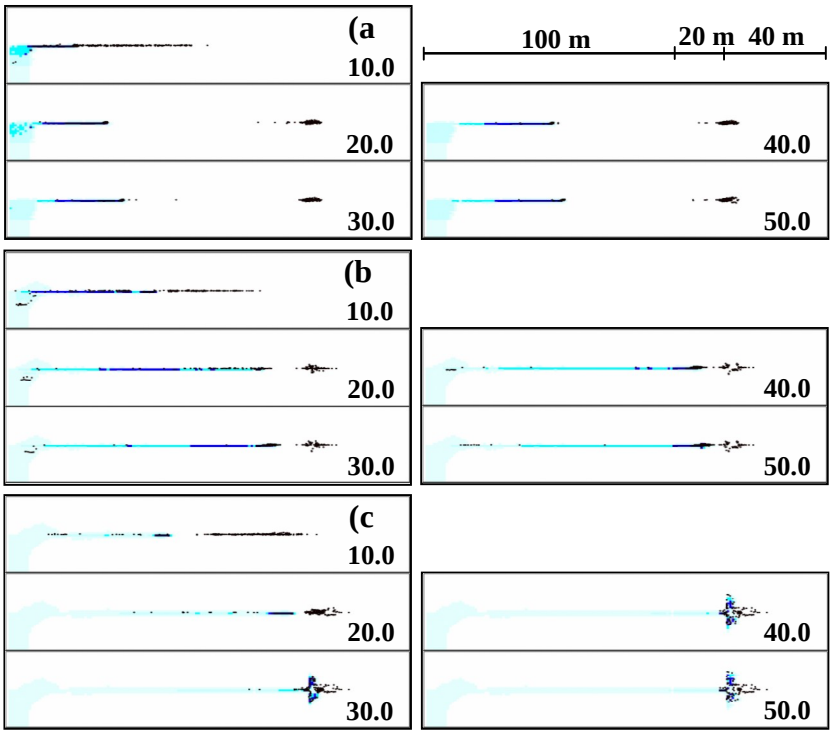

Figure 11. Effect of variations in ESP on the extent of debris flow deposition in scenario 2 for (a) case 1, (b) case 2, and (c) case 3.

3.3. Influence of the slope gradient (scenario 3)

3.3.1 Travel distance in scenario 3

The effect of a change in the slope gradient from 40° to 35° was analyzed in this scenario. All other parameters were the same as those used in scenario 1. In this scenario, the effect of a change in slope gradient was analyzed with respect to the ESP variations in the surface layer, while the sub-surface layer parameters were fixed as in case 2, scenario 1.

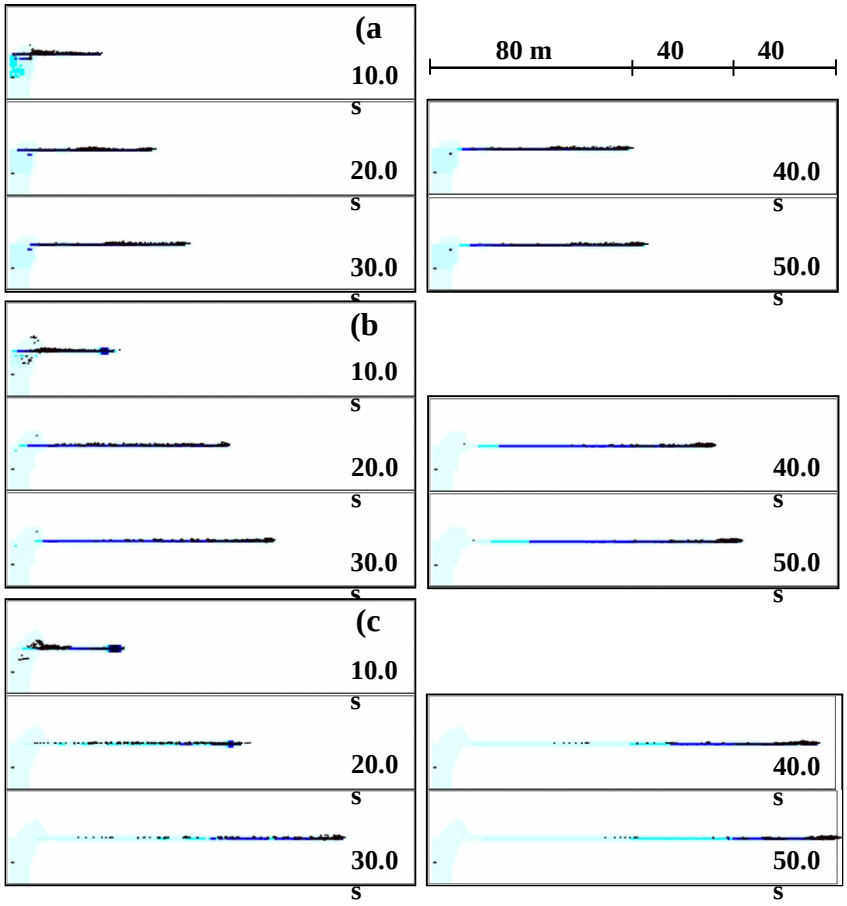

Figure 12. Effect of slope gradient on the travel distance of debris flow in scenario 3 for (a) case 1, (b) case 2, and (c) case 3.

The simulation results of debris flow run-out and the extent of deposition are displayed in Figs. 12 and 13. Figure 12 shows that the overall effect of ESP variation on the travel distance of debris flow run-out is similar to scenarios 1 and 3. The effect of a change in slope gradient from 40° to 35° on the travel distance of debris flow run-out was such that scenario 3, with a 35° slope gradient, experienced a faster and longer travel distance than scenario 1, which had a 40° slope gradient. This is because the 35° slope gradient had a thicker layer of saturated soil and a thinner layer of unsaturated soil in the sliding segment of slope failure than those in the 40° slope gradient (see Fig. 2a and c). However, the degree of saturation and the concentrations of sediment were similar in the 35° and 40° slope gradients (Figs. 3a and c; 4a and c). The maximum travel distance of debris flow for each case, as shown in Fig. 12a-c, was about 86.20 m, 122.97 m, and 161.56 m from the top

of the channel for cases 1, 2, and 3, respectively.

These results indicate that the thickness of the saturated soil layer has a significant effect on the travel distance of debris flow, just as it affects the ground water table along the slope. These results support those of previous studies (*e.g.*, Ayotte and Hungr, 2000; Chau et al, 2000; Legros, 2002), which indicated that an increasing presence of surface water and water content in the slide path enhances the mobility of debris flow.
and 2.

Comparisons between 35° and 40° slope gradients showed that the extent of deposition of debris flow in scenario 3, which had a 35° slope gradient, was similar in area to case 1 and broader in area than in cases 2 and 3, compared to scenario 1, which had a 40° slope

3.3.2 Extent of deposition in scenario 3

The extent of deposition displayed in scenario 3 (Fig. 13) shows that the earth block of cylinders moves quickly in the first 10.0 seconds. It then begins to deposit sediment about 20.0 seconds after reaching 120 m from the top of the channel, and the earth block of debris flow spreads out from this area. In fact, the general trend of the extent of the area of deposition is similar to those in scenarios 1 gradient. This is due to the effect of the thicker layer of saturated soil in the sliding segment of slope failure (Fig. 2c). These results indicate that the smaller slope gradient elevated the ground water table in the slope and affected the travel distance and the extent of the deposition of debris flow.

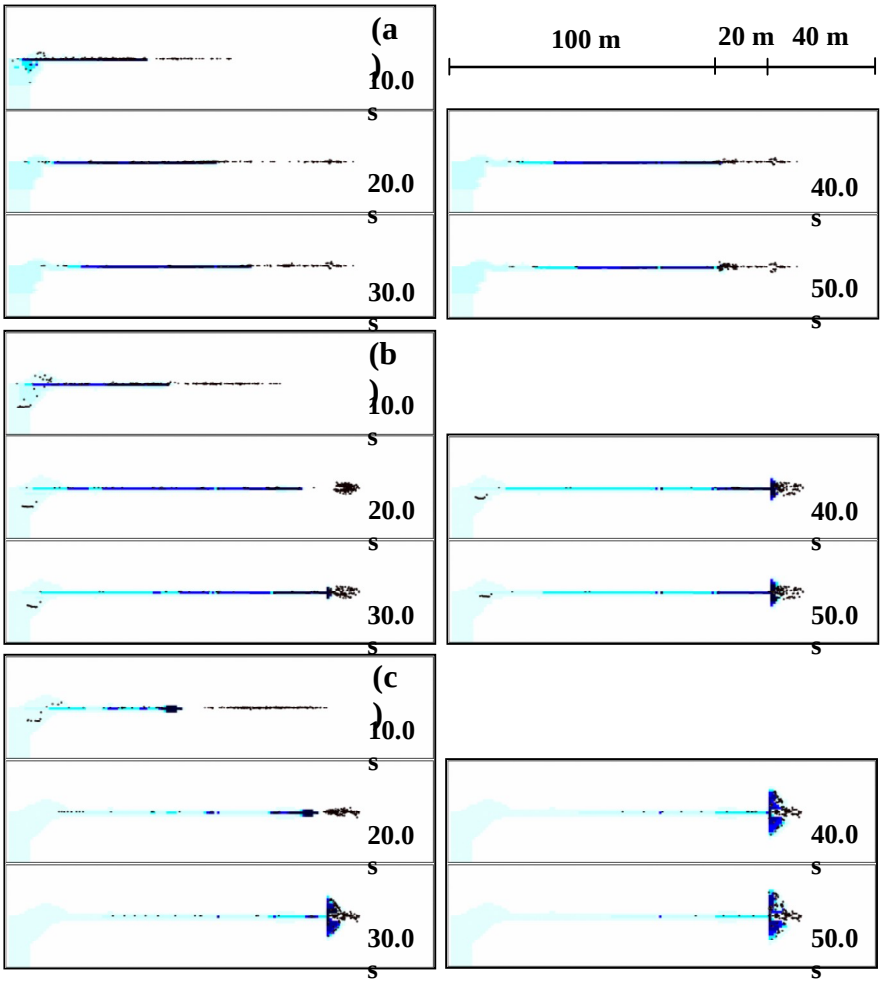

Figure 13. Effect of the slope gradient on the extent of deposition of the debris flow in scenario 3 for (a) case 1, (b) case 2, and (c) case 3.

4. DISCUSSION

Sensitivity analysis of the three main parameters in the study on the effect of ESP variations on the travel distance of debris flow run-out was performed (Table 2). The input data used in the sensitivity analysis were the same data used in scenario 1 (see Figs. 2a, 3a, and 4a).

The sensitivity analysis for the thickness of the saturated and unsaturated earth-block layers in the sliding segment of the slope was conducted first. This analysis used data from cases 1, 2, and 3 for the thickness h_{sb} and h_s of the earth block in the sliding segment of the slope (Fig. 2a), as well as data from case 2 for the degree of saturation and sediment concentrations.

Table 2. Summary of analysis of sensitivity for the study on the effect of ESP variations on the travel distance of debris flow run-out.

No.	Analysis of sensitivity	Input data of the analyzed cases		
		h_{sb}, h_s	S_b	C
1	Earth block Thickness, h_{sb}, h_s	Case 1, 2, 3	Case 2	Case 2
2	Degree of saturation, S_b	Case 2	Case 1, 2, 3	Case 2
3	Sediment concentrations, C	Case 2	Case 2	Case 1, 2, 3

Sensitivity analysis for the degree of saturation was conducted next. In this analysis, data from cases 1, 2, and 3 were used for the degree of saturation (Fig. 3a), and data from case 2 were used for the thickness h_{sb} and h_s of the earth block and the sediment concentrations. Sensitivity analysis for the sediment concentrations was conducted last. Data from cases 1, 2, and 3 were used for the sediment concentrations (Fig. 4a), and data from case 2 were used for the thickness h_{sb} and h_s of the earth block and the degree of saturation. Figures 14, 15, and 16 show the results of the sensitivity analysis of the thickness of saturated and unsaturated earth-block layers, the degree of saturation, and the sediment concentrations.

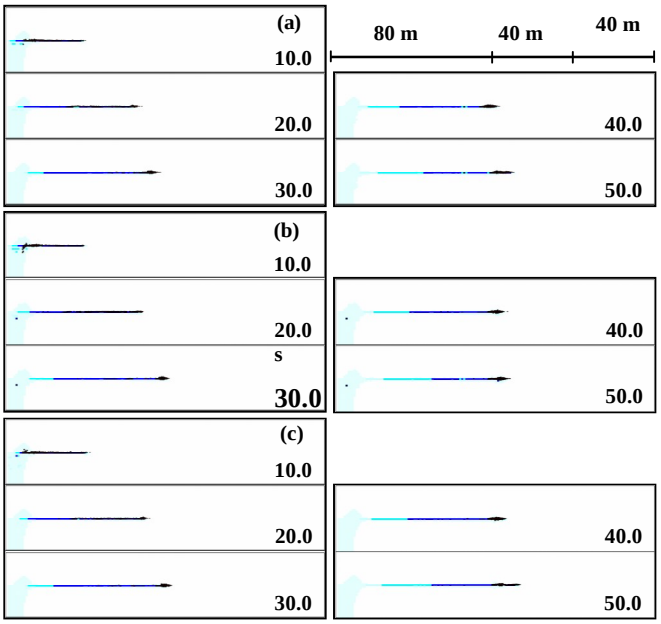

Figure 14. Sensitivity analysis of the travel distance of debris flow using the soil thickness data variations of (a) case 1, (b) case 2, and (c) case 3, as well as the fixed parameters of case 2 for the degree of saturation and the sediment concentration.

The sensitivity analysis of the thickness of saturated and unsaturated earth block layers (Fig. 14a-c) shows that the travel distance of debris flow run-out is similar in cases 1, 2, and 3 because the thicknesses of the saturated and unsaturated earth-block layers were similar within each case (see Fig. 2a). Similar conditions are shown in Fig. 15a-c for the sensitivity analysis of the degree of saturation. This figure shows that the travel distance of debris flow is similar in cases 1, 2, and 3 (see Fig. 3a).

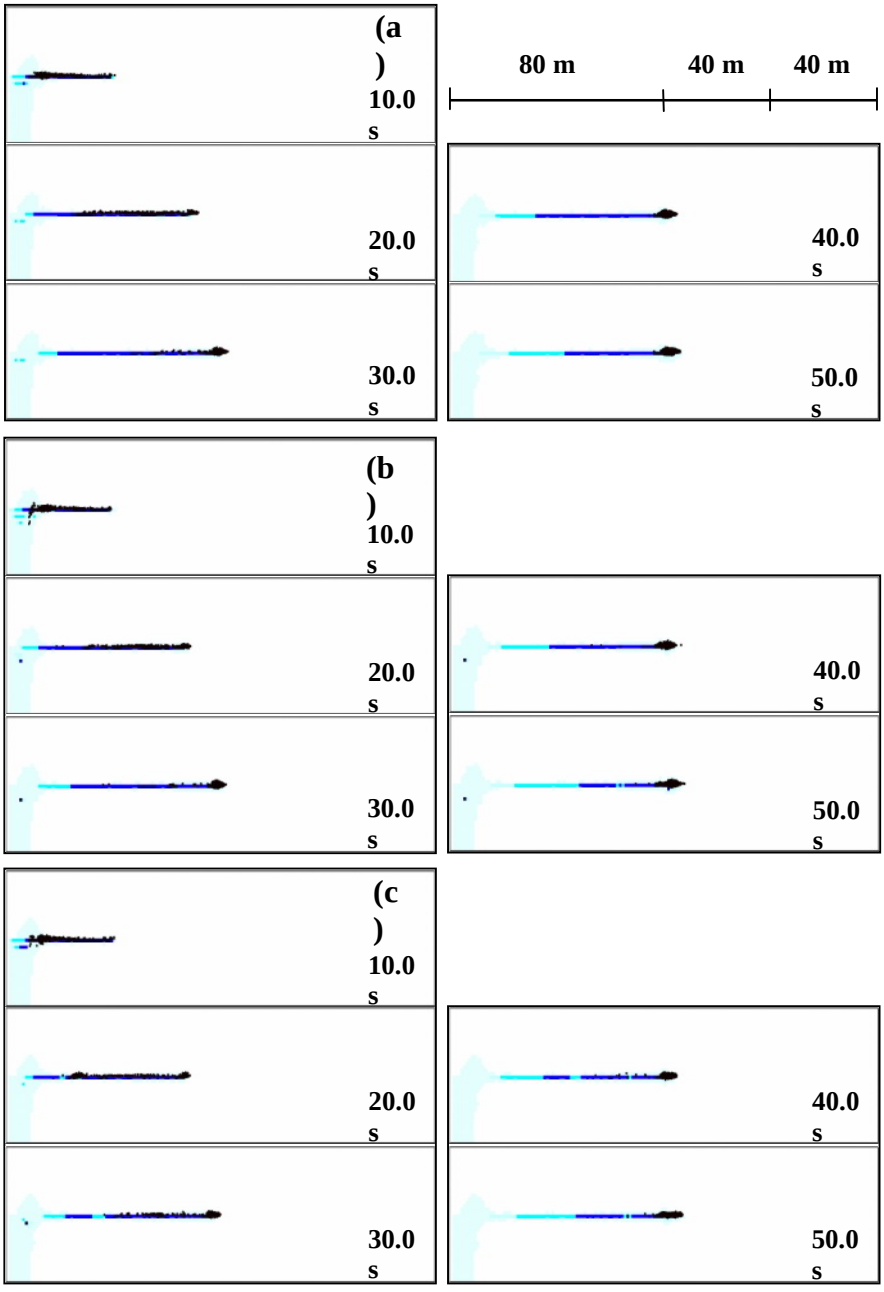

Figure 15. Sensitivity analysis of the travel distance of debris flow using the degree of saturation data variations of (a) case 1, (b) case 2, and (c) case 3, as well as the fixed parameters of case 2 for soil thickness and sediment concentration.

The sensitivity analysis of the sediment concentrations is shown in Fig. 16a-c. This figure illustrates that case 1, which had greater sediment concentrations than case 2, had a shorter travel distance of debris flow run-out. In contrast, case 3, with lower sediment concentrations than case 2, had a longer travel distance of debris flow run-out.

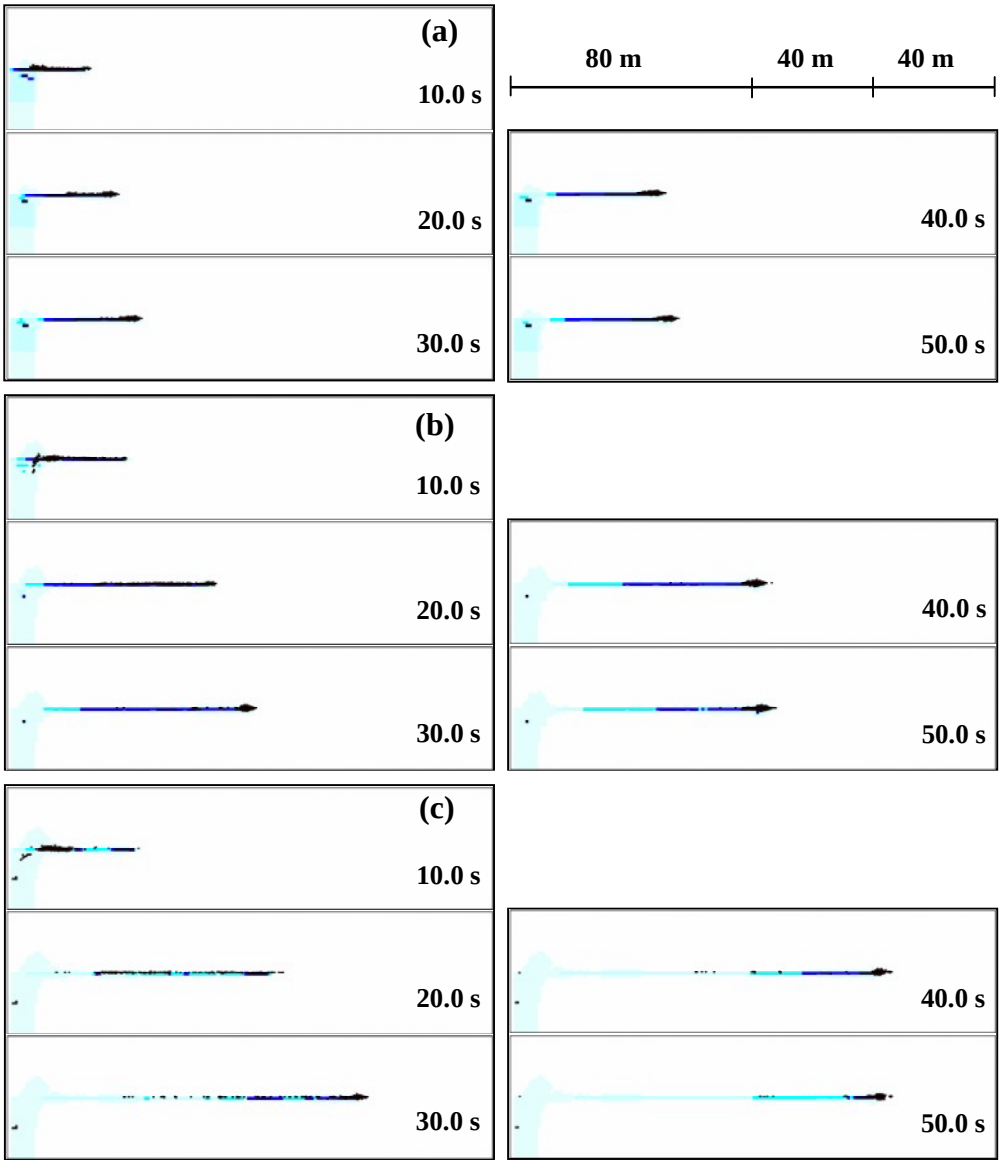

Figure 16. Sensitivity analysis of the travel distance of debris flow using the sediment concentration data variations of (a) case 1, (b) case 2, and (c) case 3, as well as the fixed parameters of case 2 for soil thickness and the degree of saturation.

The results indicate that sediment concentration has a greater effect on the travel distance of debris flow than do soil thickness and the degree of saturation. It is therefore important to parameterize ESP values, because they have a powerful effect on sediment concentration in the slope soil, thereby controlling the run-out distance of debris flow.

5. CONCLUSIONS

This study examined the effect of ESP values on the travel distance and extent of deposition of debris flow. Three scenarios of ESP variation were analyzed: scenario 1, with ESP variation only in the surface layer and a 40^o slope gradient; scenario 2, with ESP variations in both the surface and sub-surface layers and a 40^o slope gradient; and scenario 3, with ESP variations only in the surface layer and a 35^o slope gradient. Figures 8-13 show that the travel distance and extent of deposition of debris flow are simulated satisfactorily by using two-dimensional numerical models.

The results demonstrate that the three scenarios exhibited similar trends. In case 1, which had smaller ESP values than case 2, the movement of debris flow was very slow, and the travel distance of debris flow was shorter (see Figs. 8a, 10a, and 12a), because the lower ESP values resulted in a higher concentration of sediment in the slope failure area (Fig. 4a-c). In case 3, which had greater ESP values than case 2, the movement of debris flow was more rapid and the travel distance of debris flow was longer (see Figs. 8c, 10c, and Fig. 12c), because the greater ESP values resulted in a lower sediment concentration in the area of slope failure (Fig. 4a-c).

A similar trend was also seen in the extent of deposition of debris flow in each scenario. In all cases, the earth block descended rapidly during the first 10.0 seconds due to the steepness of the channel slope (*i.e.*, a 31^o slope gradient). The earth block reached the deposition area faster than the liquid layer that followed it. The extent of the deposition areas differed among cases 1, 2, and 3 due to the effect of the variation in ESP values.

In case 1, which had lower ESP values than case 2, the extent of debris flow was smaller (see Figs. 9a, 11a, and 13a). In case 3, in which the ESP value was higher than in case 2, the spread of the earth-block debris flow was longer and wider (see Figs. 9c, 11c, and 13c).

These results support the conclusion that ESP values are a dominant factor in determining the travel distance and extent of debris flow deposition. Larger ESP values, which contribute to a larger water-holding capacity in the sliding segment of slope failure, resulted in faster and longer travel distances, and in a broader extent of deposition of debris flow. As a consequence, such larger ESP values may increase the risk of damage in downstream regions. These results support those of many previous studies (*e.g.,* Iverson *et al.,* 1998; Chau *et al.,* 2000; Legros, 2002), which concluded that an increase in the water content of the debris flow materials leads to an increase in the run-out distance, and that an increase in the sediment content causes a decrease in the run-out distance.

An analysis of a change in slope gradient from 40^o to 35^o showed that in a 35^o slope gradient, the depth of the ground water table in the slope increased and led to a thicker layer of saturated soil in the slope than in a 40^o slope gradient. At the time of slope failure, a thicker saturated soil layer in the sliding segment of the slope results in a faster flow and a longer travel distance of debris flow run-out. These results match the results of Ayotte and Hungr (2000), Chau *et al.* (2000), and Legros (2002), who reported that an increase in the presence of surface water in the slide path enhances the mobility of debris flow.

REFERENCES

Ayotte, D. and Hungr, O. (2000): Calibration of a runout prediction model for debris flows and avalanches, Proceedings of the Second International Conference on Debris Flows Hazards Mitigation/Taipei/Taiwan, p.505 514, Balkema, Rotterdam

Chen, H and Lee, C.F. (2000): Numerical simulation of debrisflow. Canada Geotechnical Journal. 37. p. 146 160

Chau, K.T., Chan, L.P.T., Luk, S.T. and Wai, W.H. (2000): Shape of deposition fan and run-out distance of debris flow: Effect of granular and water content. Proceedings of the Second International Conference on Debris Flows Hazards Mitigation /Taipei/Taiwan, p.387 –395, Balkema, Rotterdam

Ghilardi, P., Natale. L and Savi, V. (2003): Experiment and mathematical simulation of debris-flow runout distance and deposition. Proceedings of the Third International Conference on Debris-Flows

Hazards Mitigation: Mechanics, Prediction, and Assessment, Davos, Switzerland, p.601 610, Millpress, Rotterdam

Hungr, O. 1995: A model for the runout analysis of rapid flow slides, debris flows, and avalanches. Canada Geotechnical Journal. 32. p. 610 623

Iverson, R.M., Schilling, S.P. and Vallance, J.W. (1998): Objective delineation of lahar-inundation hazard zones. Geological Society of America Bulletin, v.110, no. 8, p.972 984

Laigle, D., Hector, A.F, Hubl, J. and Rickenmann, D. (2003): Comparison of numerical simulation of muddy debris-flow spreading to records of real events. Proceedings of the Third International Conference on Debris-Flows Hazards Mitigation: Mechanics, Prediction, and Assessment, Davos, Switzerland, p.635 – 646, Millpress, Rotterdam

Legros, F. (2002): The mobility of long-runout landslides. Engineering Geology. 63. p. 301 331

Lorenzini, G. and Mazza, N. (2004): Debris flow: Phenomenology and Rheological Modelling. WIT press, Southampton, Boston

Mukhlisin, M., Kosugi, K., Satofuka, Y., and Mizuyama, T. 2006. Effects of Soil Porosity on Slope Stability and Debris Flow Runout at a Weathered Granitic Hillslope. Vadoze Zone Journal. 5:283-295

Nakagawa, H., Takahashi, T. and Satofuka, Y. (2000): A debris-flow disaster on the fan of the Harihara River, Japan. Proceedings of the Second International Conference on Debris Flows Hazards Mitigation/Taipei/Taiwan, p.193 –201, Balkema, Rotterdam

Okura, Y., Kitahara, H., Kawanami, A. and Kurokawa, U. (2003): Topography and volume effects on travel distance of surface failure. Engineering Geology. 67 p.243 254

Satofuka, Y and Takahashi, T. (2003): Numerical simulation of a debris flow caused by landslide. Annual Journal of Hydraulic Engineering. JSCE. 47.p.583 – 588 (in Japanese)

Takahashi, T. (2000): Newtonian and flow of various types of debris flow. Proceedings of the Second International Conference on Debris Flows Hazards Mitigation/ Taipei/Taiwan, p.15 – 25, Balkema, Rotterdam

Takahashi, T., Nakagawa, H. and Satofuka, Y. (2000): Newtonian fluid model for viscous debris flow. Proceedings of the Second International Conference on Debris Flows Hazards Mitigation/Taipei/Taiwan, p.255 – 262, Balkema, Rotterdam

Takahashi, T., Satofuka, Y. and Kashimoto, S. (2003): Motion of landslide-induced debris flow. Proceedings of the Third International Conference on Debris-Flows Hazards Mitigation: Mechanics, Prediction, and Assessment, Davos, Switzerland, p.399 410, Millpress, Rotterdam